AD-A111 766 NAVAL SURFACE WEAPONS CENTER SILVER SPRING MD F/G 20/4
AN INVISCID COMPUTATIONAL METHOD FOR TACTICAL MISSILE CONFIGURA--ETC(U)
MAY 81 A B WARDLAW, J M SOLOMON, F P BALTAKIS

UNCLASSIFIED NL

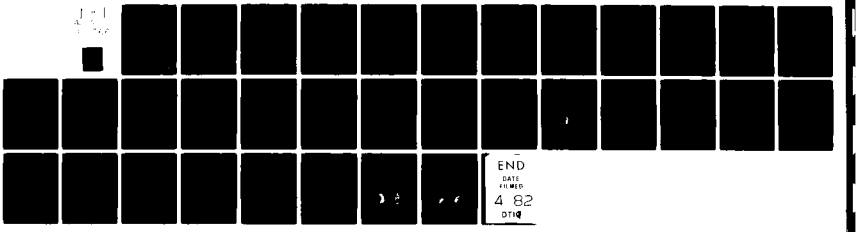

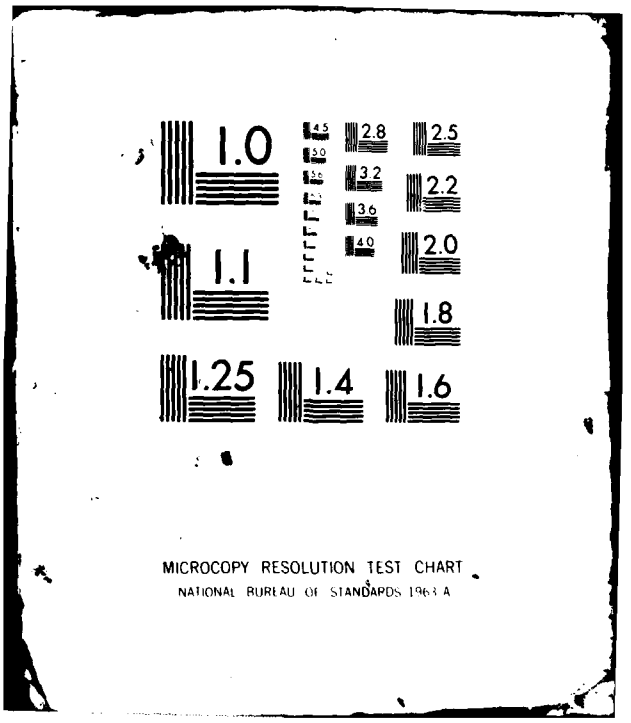
1.0
1.1
1.25
1.4
1.6
2.8
2.5
3.2
2.2
3.6
2.0
4.0
1.8
MICROCOPY RESOLUTION TEST CHART
NATIONAL BUREAU OF STANDARDS 1963 A

ADA111766

AN INVISCID COMPUTATIONAL METHOD FOR TACTICAL MISSILE CONFIGURATIONS

A. B. Wardlaw, Jr., J. M. Solomon, F. P. Baltakis and L. B. Hackerman
Naval Surface Weapons Center, Silver Spring, Maryland 20910

Abstract

14 MAY 81

A finite difference method suitable for design calculations of finned bodies is described. Efficient numerical calculations are achieved using a thin fin approximation which neglects fin thickness but retains a correct description of the fin surface slope. The resulting algorithm is suitable for treating relatively thin, straight fins with sharp edges. Methods for treating the fin leading and trailing edges are described which are dependent on the Mach number of the flow normal to the edge. The computed surface pressures are compared to experimental measurements taken on cruciform configurations with supersonic leading and trailing edges and to a swept wing body with detached leading edge shocks. Calculated forces and moments on body-wing-tail configuration with subsonic leading edges are compared to experiment also. Body alone configurations are studied using a Kutta condition to generate a lee-side vortex.

1. Introduction

A practicable means of predicting the nonlinear, inviscid, supersonic shock layer on missile configurations is to numerically solve the steady, three-dimensional inviscid equations using an efficient finite difference method. Several computer programs are currently available for this purpose, e.g. Refs. 1-7. Although these supersonic flow field codes can be applied to relatively arbitrary body shapes, their application to practical wing-body-tail configurations presents some serious computational problems. Existing codes treat the complete fin-body cross section as a single entity. Thus when cylindrical coordinates, as shown in Fig. 1, are used a large number of ϕ mesh

FILE COPY

82 03 09 064

This document has been approved for public release and sale; its distribution is unlimited.

TIC
ELECTE
MAR 8 1982
S
A

planes are needed to adequately resolve the fin. When several fins are present at the same axial station, the number of grid points needed becomes prohibitively large for practical design calculations. The number of grid points can be substantially reduced by mapping the fin body cross-section into a more "rounded" figure. The existing methods utilizing this approach are based on conformal mapping techniques developed by Moretti[2,8] (see Refs. 3,6). The mappings however are complicated even for the case of a single smooth fin or wing and often tend to cluster large numbers of mesh points near wing tips. This reduces the permissible marching step and increases computational time.

The primary focus of the present study is the development of a more efficient numerical technique for treating finned bodies. To achieve this, the approach used here departs from the basic computational strategy used in Refs. 1-7 when fin surfaces are present. Instead of considering the cross-sectional body-fin geometry as a single entity, the present approach considers the body alone (i.e., the body with all fin surfaces removed) and the fin geometry separately. The computational grid is generated using normalizing transformations [1,4,5,7] applied to the body alone configuration. The fin surfaces are allowed to extend into the computational region and can be adequately resolved within a relatively coarse computational grid. In order to treat the complex flow in the immediate vicinity of fin leading and trailing edges, appropriate local analyses are built into the program which depend strongly on the local Mach number of the flow component normal to the edge. These local analyses can range from locally exact, when the edge is sharp and the normal velocity component is sufficiently supersonic, to ad hoc or semi-empirical in other situations.

Within this framework, various approaches for numerically treating general fin surface shapes are possible. One approach would be to introduce extra

computational points to represent the fin surfaces which would float within the basic grid. This would complicate the application of the boundary conditions on the fin surfaces. Another approach, would be to subdivide the flow domain into several sub-regions each containing the flow between adjacent fin surfaces. Relatively simple transformations would be applied separately in each sub-region to map adjacent fin surfaces onto constant computational coordinate planes.

Relatively coarse meshes could be used in each sub-region and the computations in the various sub-regions could be linked in a manner suggested by Hindman, et al.[9] Both the above mentioned approaches are in principle capable of handling general fin surface geometries.

To simplify the development for the present study, the analysis is restricted to relatively thin fins with sharp edges which lie approximately along constant ϕ planes (cf., Fig. 1). A thin fin approximation is employed which neglects the fin thickness but retains the actual fin surface slopes. For an important class of body-fin configurations, the thin fin approximation allows the direct use of the basic grid generated for the body alone shape (see Sec. 2) without the introduction of floating points to describe the fin surface or additional mappings. To verify the thin fin approximation and the versatility of the computational method presented here (see Secs. 2 and 3), comparisons are made of computed and measured surface pressure distributions for body alone, body-wing and body-wing-tail configurations. A representative sampling of these is presented in Sec. 4.

2. Notation and Preliminaries

The numerical methods for treating fin body combinations presented here differ from existing supersonic inviscid flow field codes [1-7] only in the treatment of fin surfaces. In the present work, the procedures for treating

DTIC COPY INSPECTED 2

fin surfaces, which appear in Sec. 3, will be described and implemented within the context of the algorithm described in Refs. 7 and 9. However, this fin treatment can be adapted in a straightforward manner to other existing supersonic inviscid flow codes which have the capability of treating internal shock waves either by "tracking" or "capturing".

A body oriented cylindrical coordinate system (r,ϕ,z) depicted in Fig. 1 is used in this study. Standard notation will be used; viz., ρ is the density, p the pressure, h the enthalpy, a the sound speed, γ the ratio of specific heats, and $\vec{q}$ the velocity vector with components (u,v,w) as indicated in Fig. 1. It is assumed that for $z \geq z_o$, $w > a$ everywhere. For computational purposes, attention is restricted to the region $z \geq z_o$ between the body alone, expressed by $r=b(\phi,z)$ and the bow shock wave, expressed by $r=c(\phi,z)$. This region is mapped into the computational region $Z \geq z_o$, $0 \leq X \leq 1$, $0 \leq Y \leq 1$ by the standard normalizing transformations [1,4,5,7]

$$Z = z, \quad X = (r-b)/(s-b), \quad Y = \phi/\phi_o \tag{1}$$

where ϕ_o is the ϕ value of a symmetry plane if one exists and 2π otherwise. Every computational plane Z = constant is covered by a grid with uniform ΔX and ΔY. As will be described in Sec. 3, the fin cross-section is represented by the thin fin approximation as double valued grid points lying along portions of certain Y = constant grid lines; cf., Fig. 2.

The algorithm for advancing the unknown flow field quantities from $Z = Z^k$ to the next axial station $Z = Z^k+\Delta Z$ depends on the location of the individual mesh points in the shock layer. These are divided into the following four types: interior, body surface, shock, and fin surface point. The numerical procedures used to treat the first three types of points are essentially the same as those given in Refs. 7 and 9. The only difference is that the inviscid, weak conservation equations have been recast to simplify the source term. For

interior points the MacCormack predictor-corrector scheme is applied directly to the associated conservation form of these equations in the X, Y, Z space. The points on the body and bow shock surfaces are treated using predictor-corrector methods applied to certain characteristic compatibility relations for each surface along with the appropriate flow boundary conditions. See Refs. 7, 10 and 11 for complete details.

3. Computational Procedure for Fin Surfaces

The Thin Fin Approximation

The thin fin approximation is applicable to fins with surfaces that lie close to a constant ϕ plane, say $\phi = \phi_f$, which is defined as the fin plane. The fin geometry is assumed to be represented by two surfaces, the upper and lower surfaces, each described independently by relations of the form

$$\phi = \phi_f + \sigma\ (r,z). \tag{2}$$

In the cross-section Z = const., the actual fin surfaces will lie within the computational mesh as shown in Fig. 2. The thin fin approximation assumes that $|\sigma|$ is small and thus places the fin surfaces along the fin plane corresponding to $Y = Y_f$ in each Z = constant plane. Although the fin is approximated by a zero thickness plane lying on $\phi = \phi_f$, the correct description of the fin surface slope is retained. Only the fin surface slopes and their r and z derivatives are required. The derivatives of σ, correct to $O(|\sigma|)$, are given by

$$r\sigma_r = \tan\theta,\ r\sigma_z = \tan\nu,$$

$$r\sigma_{rr} = \sec^2\theta\ (\theta_r - \sigma_r) - \sigma_r$$

$$r\sigma_{zz} = \sec^2\theta\nu_z - \sigma_r \tan^2\nu,\ r\sigma_{rz} = \sec^2\theta\ (\theta_z - \sigma_z)$$

Here θ and ν are the angles between the fin surface tangency plane and the fin plane in the r and z directions, respectively Within the restriction that $|\sigma|$ be "small", the thin fin approximation can be applied to arbitrary fin geometries including surfaces with discontinuous slopes and fins with "small"

deflections, camber, and variations in dihedral.

The Numerical Procedure For Fin Surfaces

The numerical algorithm for treating fins by the thin fin approximation requires that the computational mesh be chosen so that each fin plane is coincident with a computational mesh plane, $Y = Y_f$. Two sets of computational points are carried on the $Y = Y_f$ plane to describe the flow properties on the upper and lower surfaces, (cf., Fig 2). As the calculation is marched down the length of the body, fin surfaces are encountered on $Y = Y_f$. Thus a point at some X may at one axial location be an interior flow field point and in the next axial step move onto the fin. The interior point is split into two points corresponding to the upper and lower fin surfaces. The fin points thus created are referred to as leading edge points. For a fixed X, a pair of points which are on the fin at one axial step can in the next step move off the fin and become a single interior flow field point. Such a point will be referred to as a trailing edge point. The flow variables at leading and trailing edge points are determined from an appropriate local analysis which is described in the following subsections. The adjustment for the presence of a leading or trailing edge is made immediately after the completion of the step in which the edge is encountered. The values of the flow variables prior to the adjustment are termed "upstream" while the adjusted values are termed "downstream".

All points on the fin surfaces not designated leading or trailing edge points are advanced using certain characteristic compatibility relations and the tangent flow boundary condition as described in Ref. 11. These relations are evaluated numerically within the framework of the thin fin approximation by placing all fin surface flow quantities on the fin plane and making all evaluations at the fin plane. The juncture of the fin and the body is assumed

to be a sharp corner where the flow velocity is directed along the corner. This condition and special characteristic relations[11] are used to advance the points along the juncture. Discontinuities in the fin surface slope are explicitly treated using essentially the same techniques as those for treating discontinuities in the body surface slopes given in Refs. 7 and 10 with appropriate modifications to account for the form of (2) defining the fin surface.

Leading Edge Points

The downstream flow properties at leading edge points are determined by a local analysis based on the computed flow upstream of the edge and the prescribed local fin geometry. Using this information, the Mach number normal to the leading edge, Mn, is determined. If Mn > 1 an attached shock or expansion fan occurs in most cases which permits a local analysis (see, e. g. Chapter XI, of Ref. 12). The velocity component tangent to the edge, is unaffected by the edge and all other downstream flow quantities are determined by turning the normal flow component using either an oblique shock or a Prandtl-Meyer expansion. A similar procedure for the case of an attached oblique shock has also been used in Ref. 6. In Ref. 6, the leading edge shocks are "tracked" downstream of the edge whereas in the present work these shocks are "captured" using the conservative and dissipative properties of the interior point scheme without additional numerical smoothing.

At leading edges where a compression turn is required, the condition $M_n > 1$ does not guarantee the existence of an attached oblique shock. For sufficiently large turning angle, δ, a detached shock wave will be present and a purely local analysis is, at best, an approximation. However, it has been possible to formulate empirical rules for determining reasonable leading edge

conditions. This procedure predicts an effective shock angle which is used to turn the normal flow component and assigns the streamline direction at the leading edge. When a detached shock occurs, the upper and lower fin surfaces are treated independently of one another. If one surface permits either an attached shock or a Prandtl Meyer expansion this procedure is applied as described above. Such an approach is suggested by the experimental data of Ref. 13. When the upstream flow crosses the edge with $M_n < 1$, the flow at the leading edge is free of shock waves. On an expansion surface the flow is accelerated to sonic velocity and then turned into the plane of the wing using a Prandtl-Mayer expansion. A compression surface is treated by isentropically compressing the flow to an empirically determined Mach number and specifying a streamline direction.

On highly swept wings,which form strong leeside vortices,M_n is usually small (i.e. $M_n << 1$) or negative. On such configuration the streamlines flow outwards at wing tip,and leading edge pressure and density values are set equal to those at the adjacent wing point while the resulting velocity vector is directed along the wing tip.

For the leading edge points at the fin-body juncture a special procedure is required. The flow in the vicinity of these points features a complicated shock interaction pattern which probably cannot be resolved within the relatively coarse mesh used in the present calculations. Accordingly, a simple heuristic procedure is used to determine the flow variables immediately downstream of the leading edge corners. The upstream velocity vector on the body lies in the body tangency plane which also contains the corner direction. The flow downstream of the leading edge corner is obtained by rotating the velocity vector within the body tangency plane and aligning it with the corner using either the oblique shock or the Prandtl-Meyer turning realtions.

The technique of applying a local analysis at the leading edge is employed to improve the quality and robustness of the solution near the leading edge and thus to enhance the use of coarse grids. At a sufficiently large number of steps away from the edge, the influence of the conditions employed at a leading edge will disappear and all treatments result in similar flow fields. In certain situations it is difficult to determine reasonable leading edge conditions. Accordingly, the strategy of marching directly across the leading edge without applying a leading edge adjustment has been used. This approach works well as long as the pressure rise at the leading edge is restricted to less than a factor of two.

Trailing Edge Points

At a trailing edge the two points on $Y = Y_f$, representing the upper and lower fin surfaces, are coalesced into a single interior flow field point. A local analysis is used to determine the flow downstream of the edge from the computed flow on each fin surface upstream of the edge and the given local fin geometry.

One approach, described in Ref. 11, consists of turning the normal flow component from both surfaces, using an oblique shock and Prandtl-Meyer expansion, onto a plane containing the trailing edge. The orientation of this plane is iteratively determined by requiring that pressure on both surfaces be equal. The conditions on both sides of this plane are then averaged to produce the conditions at the coalesced interior flow field point. Such a procedure can be applied only where M_n is sufficiently large to assure the existence of the necessary oblique shocks. In practice it has been found that averaging the upper and lower surface at the trailing edge without using the iterative process to determine pressure does not change computed results significantly. This shorter process is currently used whenever the trailing edge is supersonic. At subsonic trailing edges an averaging process is used

but the interior flow point on the fin plane and adjacent to trailing edge point is included in the average.

Special Differencing Procedures

Special treatment is provided for advancing the outermost grid point on the fin surfaces, at say $X = X_\ell$, and the adjacent interior flow point, $X_{\ell+1} = X_\ell + \Delta X$. The MacCormack scheme for advancing the interior flow point, $X_{\ell+1}$, must be modified since there are two sets of flow values at X_ℓ corresponding to the upper and lower fin surfaces. The present procedure is to advance the flow variables at $X_{\ell+1}$ by the basic interior point scheme using the flow values at X_ℓ corresponding to the upper surface and then repeating the calculation at $X_{\ell+1}$ using the lower surface values at X_ℓ. The two values of the conservation vector, U, are then averaged at the end of the predictor and corrector step to obtain the final value of U at $X_{\ell+1}$. The outermost fin points are advanced using the interior flow values at $X_{\ell+1}$.

An alternate strategy is to use one sided differences to advance the interior point at $X_{\ell+1}$. If this option is used the outermost fin point is also advanced without wing information at $X_{\ell+1}$. Differences in the X direction which would normally be formed using properties at X_ℓ and $X_{\ell+1}$ are set to zero. This option is used in most cases which use a local analysis at the leading edge.

Special Y differencing procedures are also applied downstream of leading edges which feature attached shock waves. It has been found in example calculation on two dimensional rectangular fins that the standard procedure for advancing the fin surface points predicts inaccurate surface pressures immediately downstream of such discontinuities. In this region, the Y differences used to advance the fin surface flow variables must be taken across the oblique shock generated by the leading edge and these Y differences will be unrealistic for a few steps following the formation of a leading edge

point. To circumvent this problem, the Y differences used in the fin surface calculation are multiplied by a factor which is zero at the leading edge and increases to unity after a few steps. The selection of the number of steps for which the Y derivatives are damped is based on the values of the Y derivative at the leading edge and on an estimate of the number of steps required for the shock to move out to the adjacent row of points.

In a number of the examples to be discussed, calculations will feature large body or tip vortex. When such cases are run on fine grids it is necessary to add dissipation to the interior flow, body and wing surfaces. This is accomplished using a Shuman filter with a density switch.[16]

4. Numerical Results

The results computed with the present code are presented in this section and compared with the experimental data. The investigated cases consist of body alone, body-wing, body-tail and body-wing-tail configurations. The wing and tail surfaces have sharp leading and trailing edges which feature normal velocity components that range from subsonic to supersonic. All computations assume a perfect gas with $\gamma = 1.4$. The computations are started near the body vertex using a numerically generated conical flow field (see ref. 11).

Inviscid calculations for the body alone configuration at high incidence produce a leeside crossflow shock which is not present in the experimental flow field. A more realistic leeside flow field can be generated by applying an additional boundary condition, or Kutta condition, near the experimentally observed separation point. This destroys the crossflow shock and produces a leeside recirculation region or a vortex which is in agreement with experimental observations. In the current study the separation point is specified as a function of distance along the body. The separation location generally falls between two surface grid points and both of these points are specially treated.

The basic presumption in specifying properties at these points is that the velocity at the separation point should be oriented along the separation line and that pressure and density should vary smoothly across the separation line. The resulting flow field is illustrated in Fig. 3 and is qualitatively similar to the results of Oberkampf[15], which are also shown. Similar numerical results have been obtained by Klopfer and Nielsen[16] although their method of specifying the Kutta condition differs from that outlined above.

A comparison of calculated and measured surface pressures is given in Fig. 4 using the experimental data of Perkins and Jorgensen.[17] Pressure profiles have been computed with and without use of the Kutta condition. Clearly, application of the Kutta condition improves the agreement between calculation and experiment.

In Ref. 18 a tangent ogive body, equipped with tail fins of several different planforms, is tested in supersonic flow. Numerical results have been compared to experimentally measured surface pressures taken at Mach 3.7 for configurations featuring clipped delta and cranked tail fins. Both types of fins feature surface slope discontinuities at various locations along the surface. The freestream Mach number is sufficiently large to allow an attached shock solution at the fin leading edge in almost all cases. Calculated and measured surface pressures are compared for the cranked dalta wing in Fig. 5 and are in reasonable agreement. The scatter in the experimental data is a result of plotting experimental measurements from several different runs. On fin surfaces, which feature strong leading edge shocks, the leading edge pressure is over-predicted at the root and the calculated pressure jumps, occurring at the various surface discontinuities, also tend to be greater than experimental values. The thick corner boundary layer and the complex leading edge shock-body boundary interaction, presumably, have a large influence on the corner and

account for much of this discrepancy. Another area of disagreement occurs along the tip. Here predicted and measured pressures are of similar value, but the experimental pressure profile features a negative slope, while the numerical pressure distribution is almost constant. It is not clear whether this discrepancy is due to viscous phenomena. On fin surfaces which have a weak leading edge shock (or expansion) the predicted and measured fin tip pressure profiles are in good agreement. Also, the leading edge pressure at the corner is close to the experimental value. Over the entire span, calculated pressures on the trailing edge panel tend to be less than measured, probably reflecting the existence of a very thick boundary layer or separation.

Wind tunnal tests on the swept wing configurations of Ref. 19 (see Fig. 6) offer an opportunity to compare calculation with experiment for cases where detached shock waves are predicted to occur. Calculations have been compared to experiment at the Mach numbers of 2.96, 3.95 and 4.5, and at angles of attack of 0^o, $\pm 2^\sigma$, $\pm 4^\sigma$ and $\pm 6^o$. (Here positive and negative incidence refers to the windward and leeward wing surfaces respectively). The body-wing geometry, and sample results are shown in Fig 6&7. These indicate that the current computations accurately reflect changes in Mach number and angle of attack.

The data of Ref. 19 also include pressure measurements along a pitch plane body meridian. At positive incidences the instrumented ray is on the windward side of the body while at negative incidences it is on the lee-side. These measurements are compared to numerical results at an incidence of 6^o, 0^o and -6^o in Fig. 8 for a Mach number of 2.96. At $\alpha = 6^o$ the body alone data are in good agreement. The influence of the wing on the body causes an increase in the experimentally measured pressure. This increase is

correctly reflected by the calculations, but the peak predicted values are located approximately one caliber downstream of the measured ones. At an incidence of 0^{o}, the same trend is visible but the lagging appears to be somewhat less. When the angle of attack is changed to -6^{o}, the presence of the wing causes a decrease in body pressure. In this case, the body alone calculation does not agree well with experiment, presumably due to viscous effects. The body features a decreasing diameter near the base which undoubtedly results in changes in the effective body shape due to boundary layer thickening or separation. The calculated flow field features a crossflow shock near the base which produces an increase in the leeward meridian pressure profile. The numerical results for the body-wing configuration are much closer to experiment and feature the correct downward change in the body surface pressure. The predicted onset of the wing influence on the leeward meridian body pressure does not appear to lag the experimentally measured one.

On Fig. 9 additional comparisons are shown of computed and measured surface pressures for a delta planform wing-body configuration for which detached leading edge shock is predicted. The configuration features a 6-percent thick, double-wedge wing at Mach 2.86 at an angle of incidence of 8.6^{o}. Experimental measurements[20] were available along several span-wise locations and are in agreement with present computations.

Normal force and moment prediction for an airplane type configuration is illustrated on Fig. 10. The computations were performed at Mach 2 at angle of incidence of 10^{o} and are in good agreement with experiment.[21] The influence of the tail is also predicted correctly. The wing and tail surfaces of this configuration were essentially flat and had attached leading and trailing edge shocks.

On Fig. 11 computed normal force and center of pressure coefficients are compared with experiment[22] for an ogive-cylinder body with a cruciform type wing and tail surfaces. Three wing planforms, yielding different leading edge sweep angles, are included along with delfected and undeflected tail surfaces. The comparison is made at Mach 2.86 at incidences of 6^{o} and 12^{o}, providing subsonic leading edge conditions for all three wing planforms.

The computed normal force and center of premure values are in reasonable agreement with experiment for all three wing planforms. Variation in wing aspect ratio produces a monotonic change in the computed normal force coefficient. This is contrary to experimental results in which the minimum value is yielded by a wing with an intermediate aspect ratio. Presumably , the non-linearity in experimental results is due to the influence of the leeside vortex which is not modeled with sufficient accuracy in the computations.

The computed crossflow velocities for the wing of the minimum aspect ratio is qualitatively illustrated on Fig. 12. No experimental data were available for comparison.

6. Concluding Remarks

A numerical method has been developed which predicts the inviscid supersonic flow field about finned configurations of engineering interest. The computational requirements are generally modest. For example, the wing-body and cruciform body-tail cases, examined in the preceding sections, nominally required 3 and 7 minutes respectively of CPU time on a CDC 6500. The present study differs from previous methods by treating the fin and body geometries separately. At present, a thin fin approximation is employed which limits the applicability of the computational procedure to relatively slender fins with sharp leading edges. The fins must approximately lie along planes which intersect at a line inside the missile body. With this formulation it is possible to treat a wide variety

of configurations of engineering interest which can feature an arbitrary number of fins and tails containing small deflection, camber or variation in dihedral. By appropriate modeling at wing tips and at estimated body separation points, it appears feasible to simulate flow field vortices.

Acknowledgement

This work was jointly supported by the Naval Sea Systems Command and the Naval Air Systems Command. The authors would also like to acknowledge the enthusiastic support of Frank Moore of the Naval Surface Weapons Center, Dahlgren, VA., throughout the course of this investigation.

REFERENCES

1. Thomas, P. D., Vinokur, M., Bastianon, R., and Conti, R. J., "Numerical Solution for Three-Dimensional Inviscid Supersonic Flow," AIAA J., Vol. 10, No. 7, 1972, pp. 887-894.
2. Moretti, G., Grossman, B., and Marconi, F., "A Complete Numerical Technique for the Calculation of Three-Dimensional Inviscid Supersonic Flows," AIAA Paper 72-192, San Diego, Calif., 1972.
3. Marconi, F. and Salas, M., "Computation of Three Dimensional Flows About Aircraft Configurations," Computers and Fluids, Vol. 1, 1973, pp. 185-195.
4. Kutler, P., Reinhardt, W. A., and Warming, R. F., "Multishocked, Three-Dimensional Supersonic Flowfields with Real Gas Effects," AIAA J., Vol. 11, No. 5, 1973, pp. 657-664.
5. Kyriss, C. L. and Harris, T. B., "A Three-Dimensional Flow Field Computer Program for Maneuvering and Ballistic Re-entry Vehicles," Tenth USN Sym. on Aeroballistics, July, 1975.
6. Marconi, F., Salas, M., and Yaeger, L., "Development of a Computer Code for Calculating the Steady Super/Hypersonic Inviscid Flow Around Real Configurations, Vol. I-Computational Techniqeus", NASA CR 2675, April, 1976.
7. Solomon, J. M., Ciment, M., Ferguson, R. E., Bell, J. B., "Inviscid Flowfield Calculations for Reentry Vehicles with Control Surfaces," AIAA J., Vol. 15, No. 12, 1977, pp. 1742-1749.
8. Moretti, G., "Conformal Mappings for Computation of Steady, Three-Dimensional, Supersonic Flows," Numerical/Lab. Computer Methods in Fluid Dynamics, ASME, 13, 1976.

9. Hindman, R. S., Kutler, P., Anderson, D., "A Two-Dimensional Unsteady Euler-Equation Solver for Flow Regions with Arbitrary Boundaries," AIAA Paper 1465, Williamsburg, VA., 1979.

10. Solomon, J. M., Ciment, M., Ferguson, R. E., Bell, J. B., and Wardlaw, A. B., "A Program for Computing Steady Inviscid Three-Dimensional Supersonic Flow on Reentry Vehicles, Vol. 1: Analysis and Programming," Naval Surface Weapons Center/White Oak, Silver Spring, MD., NSWC/WOL TR 77-28, Feb. 1977.

11. Wardlaw, A. B., Solomon, J. M., and Baltakis, F. P., "Supersonic Inviscid Flowfield Computations of Missile Type Bodies", AIAA Paper 80-0271, Pasadena, Calif., Jan. 1980.

12. Landau, L. D. and Lifshitz, E. M., Fluid Mechanics, Pergamon Press (Addison-Wesley), 1959.

13. Ferri, A., "Supersonic Flows with Shock Waves," in General Theory of High Speed Aerodynamics, High Speed Aerodynamics and Jet Propulsion, Vol. 7, Ed.: W. R. Sears, Princeton University Press, 1954.

14. Harten, A. and Zwas, G. "Switched Numerical Shuman Filters for Shock Calculations" Journal of Engineering Mathematics, 6, 2, April. 1972, pp. 207-216.

15. Oberkampf, W. L. and Bartel, T. J., "Supersonic Flow Measurements in the Body Vortex Wake of an Ogive Cylinder" AFATL-TR-78-127, November 1978.

16. Klopfer, G. H. and Nielsen, J. N. "Euler Solutions of the Body Vortices of Tangent Ogive Cylinders at High Angles of Attack and Supersonic Speeds" AIAA Paper 81-0361.

17. Perkins, E. W. and Jorgensen, L. H."Comparison of Experimental and Theoretical Normal Force Distributions (Including Reynolds Number Effects) on an Ogive Cylinder Body at Mach Number 1.98",NACA TN 3716, May 1956.

18. Lamb, M., Sawyer, W. C. Wassum, D. L., Babb, C. D., "Pressure Distributions on Three Different Cruciform Aft-Tail Control Surfaces of a Wingless Missile at Mach 1.60, 2.36 and 3.70," Vol. II and III, NASA TM 80097, August 1979.

19. Jackson, C. M., Jr. and Sawyer, W. C., "A Method for Calculating the Aerodynamic Loading on Wing-Body Combinations at Small Angles of Attack in Supersonic Flow," NASA TN D-6441, 1971.

20. Jernell, L. S., "Comparisons of Theoretical and Experimental Pressure Distributions over a Wing-Body Model at Supersonic Speeds," NASA TN D-6480, Sept. 1971.

21. Jorgensen, L. H. and Nelson, E. R., "Experimental Aerodynamic Characteristics for Slender Bodies with Thin Wings and Tail," NASA TMX-3310, March 1976.

22. Spearman, M. L. and Sawyer, W. C., "Longitudinal Aerodynamic Characteristics at Mach Numbers from 1.6 to 2.86 for a Fixed-Span Missile With Three Wing Planforms" NASA TM 74088, Nov. 1977.

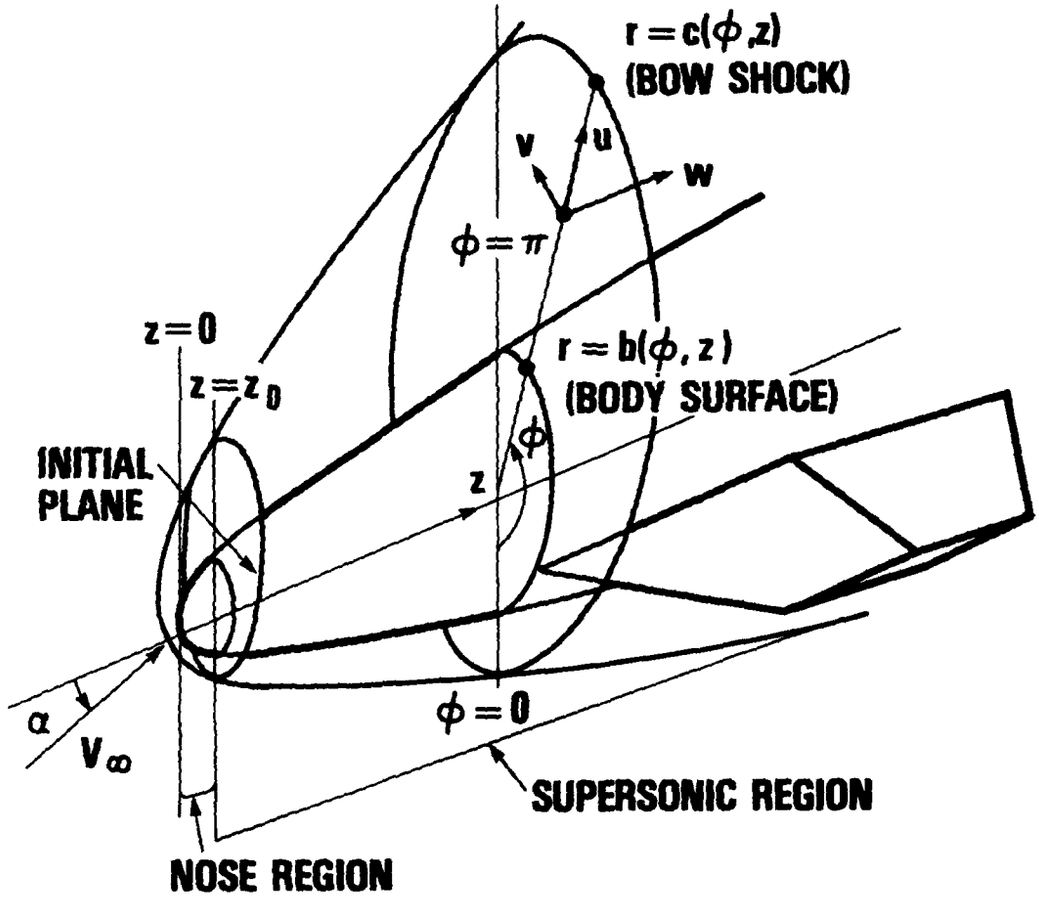

Figure 1. Cylindrical coordinate system used for inviscid flow calculation.

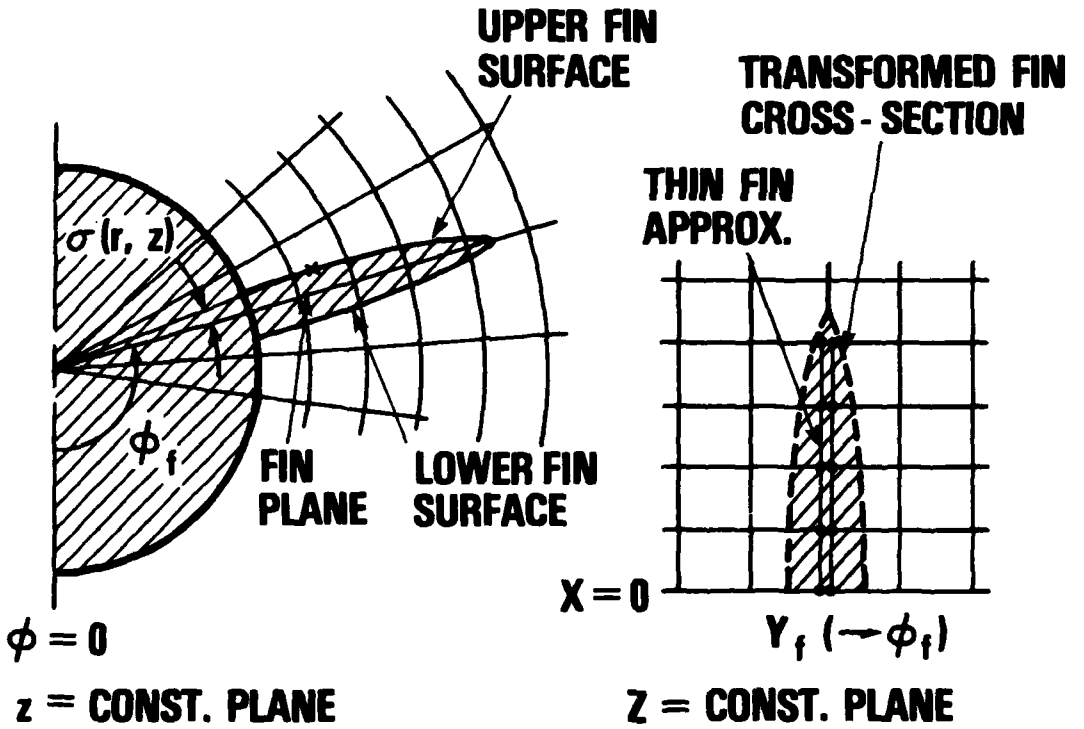

Figure 2. Cross-section view of the thin fin approximation.

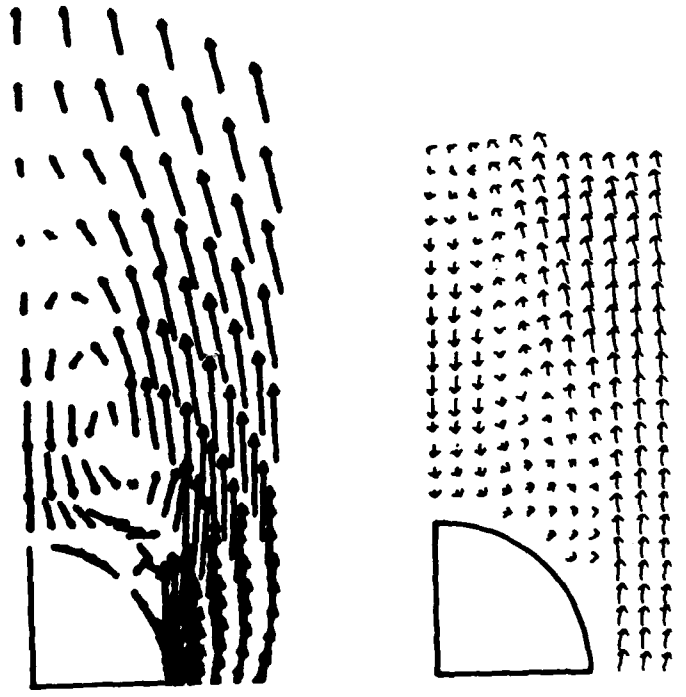

Figure 3. Calculated and measured crossflow fields on a tangent ogive at Mach 3., $RE_D = 1.7(10^6)$, $\alpha = 15^o$.

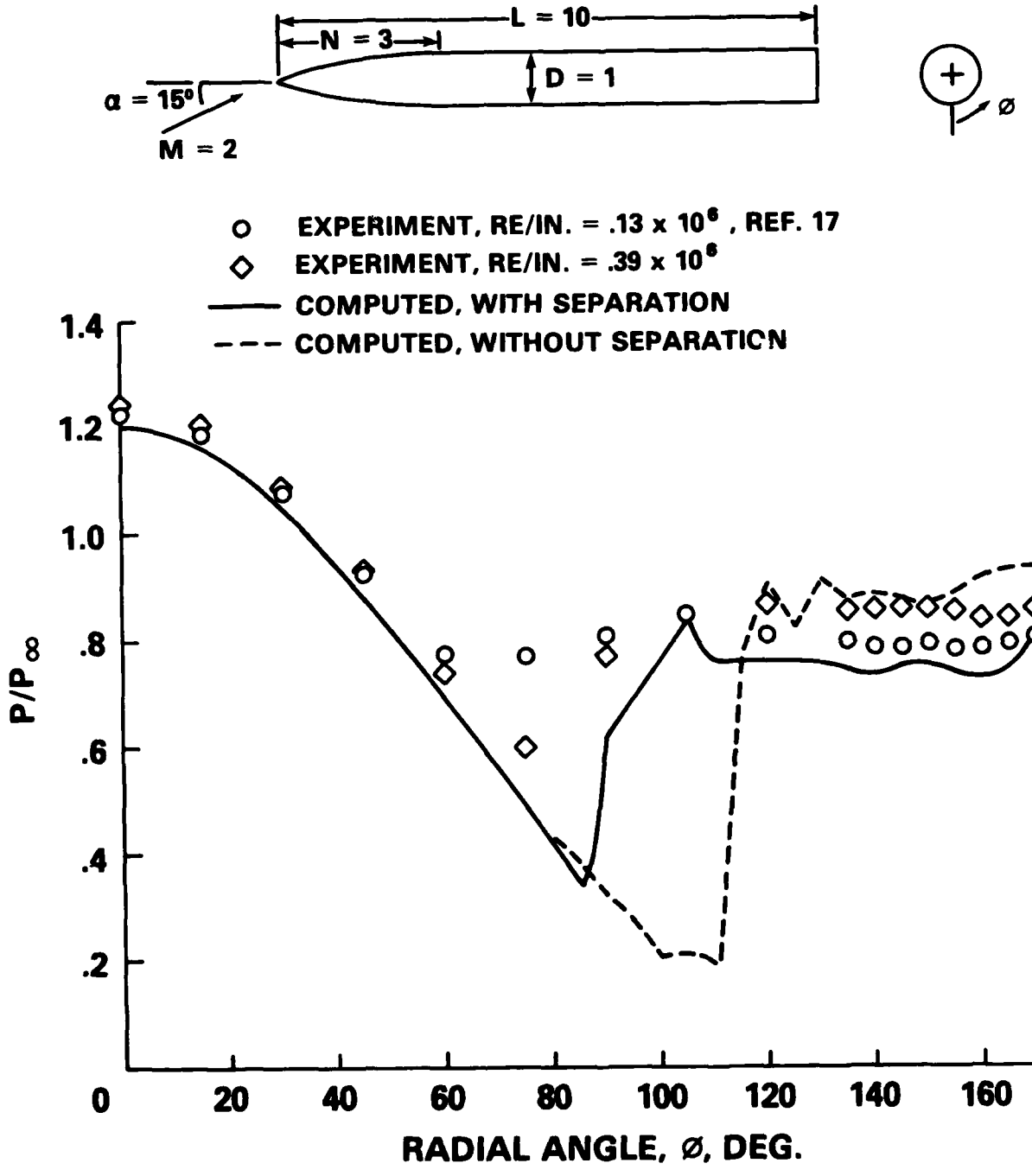

Figure 4. Calculated and measured surface pressures on a tangent ogive at Mach 2.

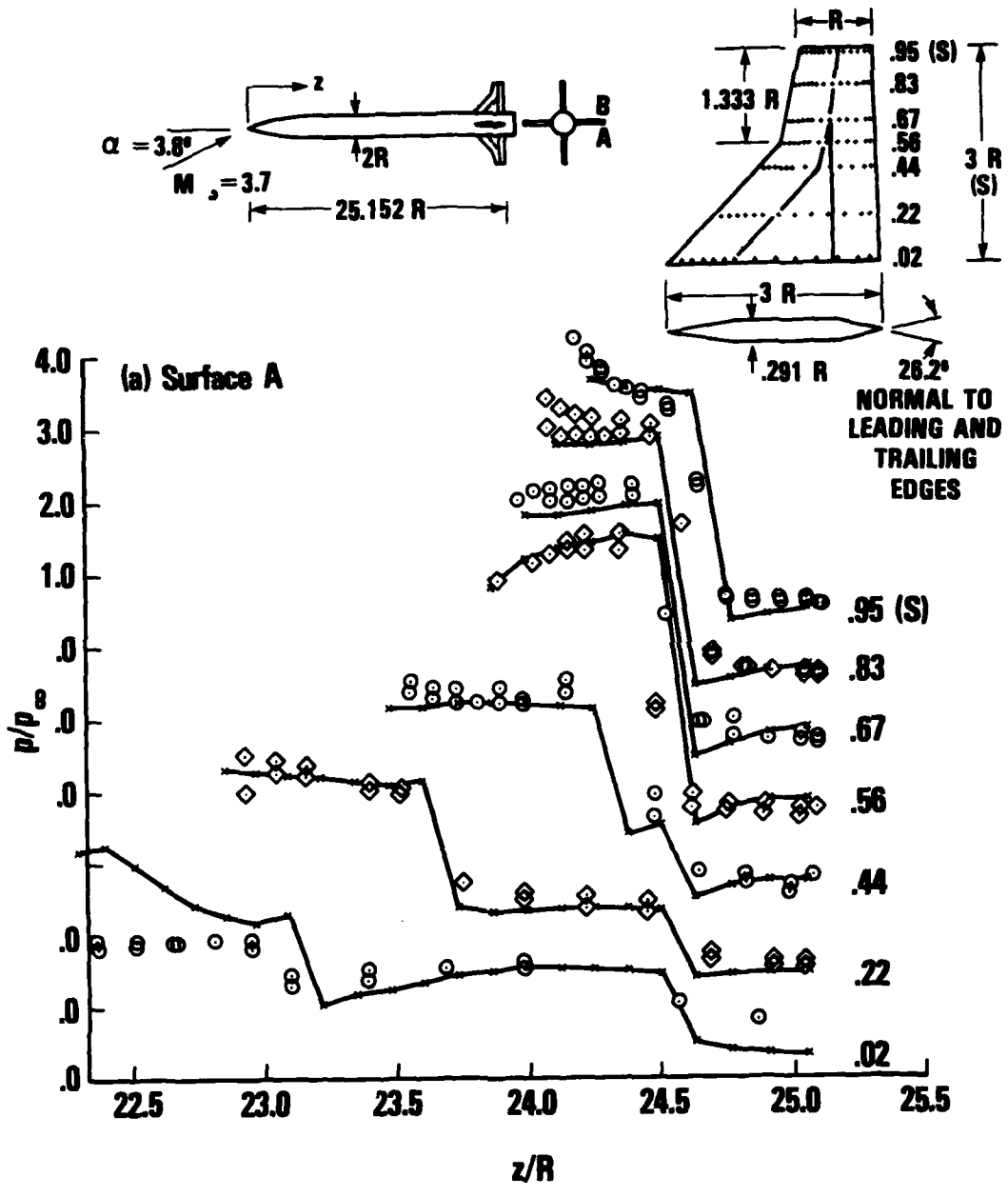

Figure 5. Comparison of computed and measured fin surface pressures on the cranked tail configuration at Mach 3.7, at $\alpha = 3.8^{\circ}$.

a. Surface A

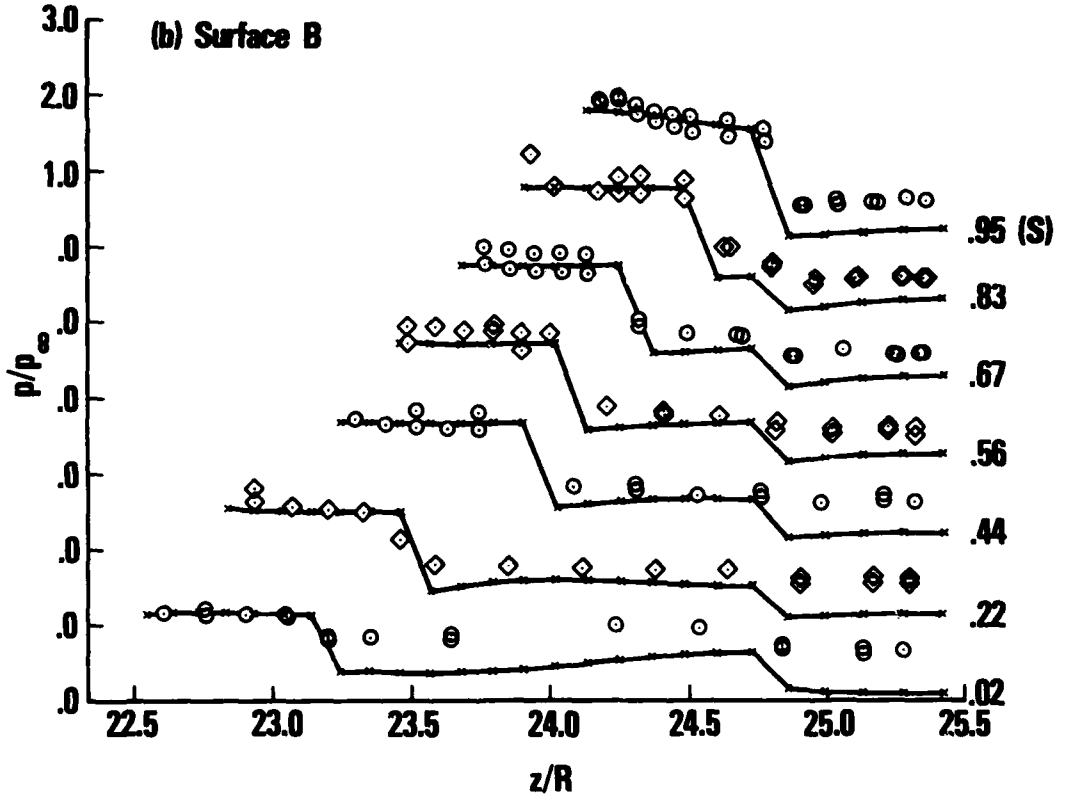

Figure 5. (Continued)

b. Surface B

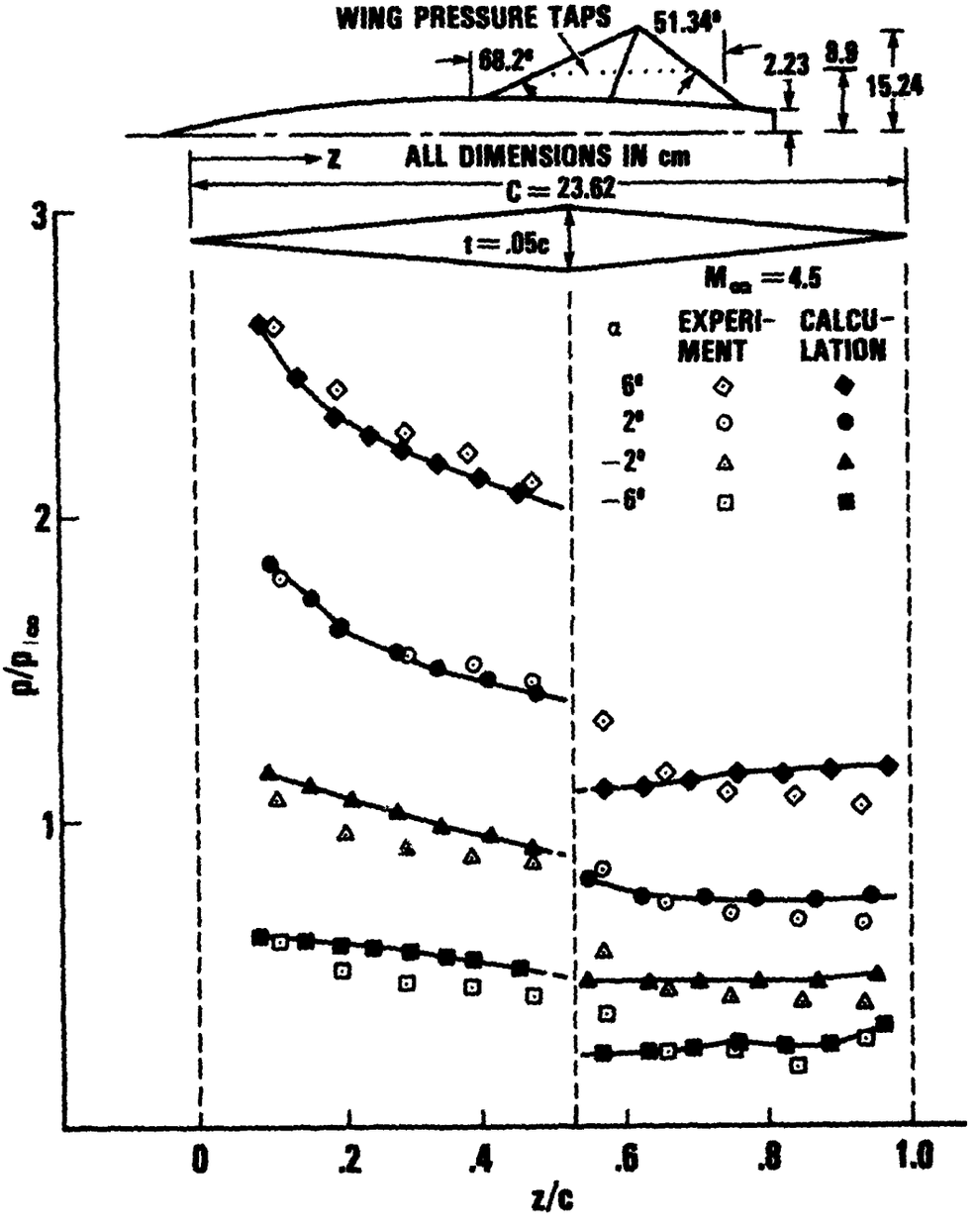

Figure 6. Comparison of computed and measured fin surface pressure as a function of incidence at Mach 4.5.

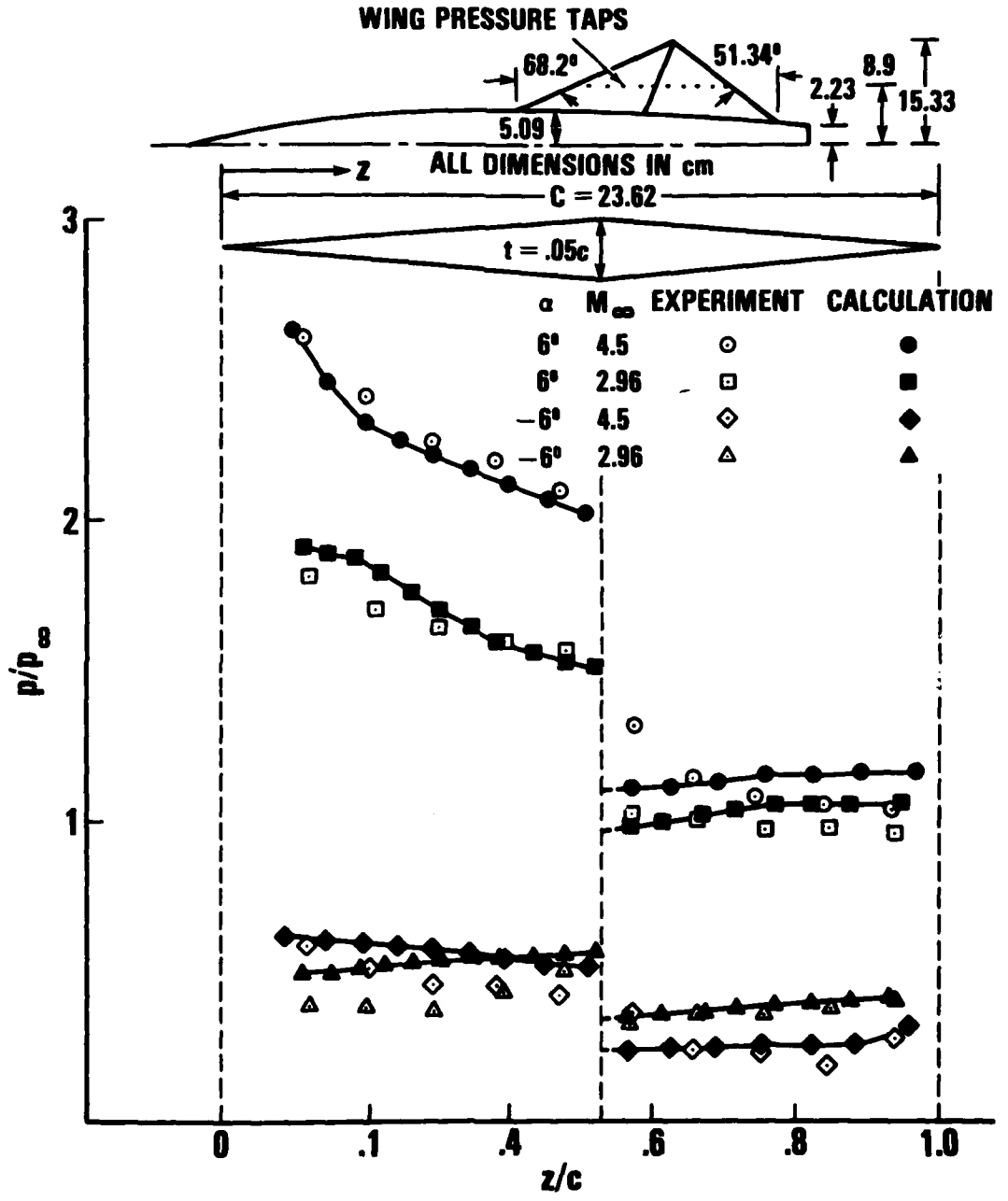

Figure 7. Comparison of computed and measured fin surface pressures at varying Mach numbers at $\alpha = \pm 6^{o}$.

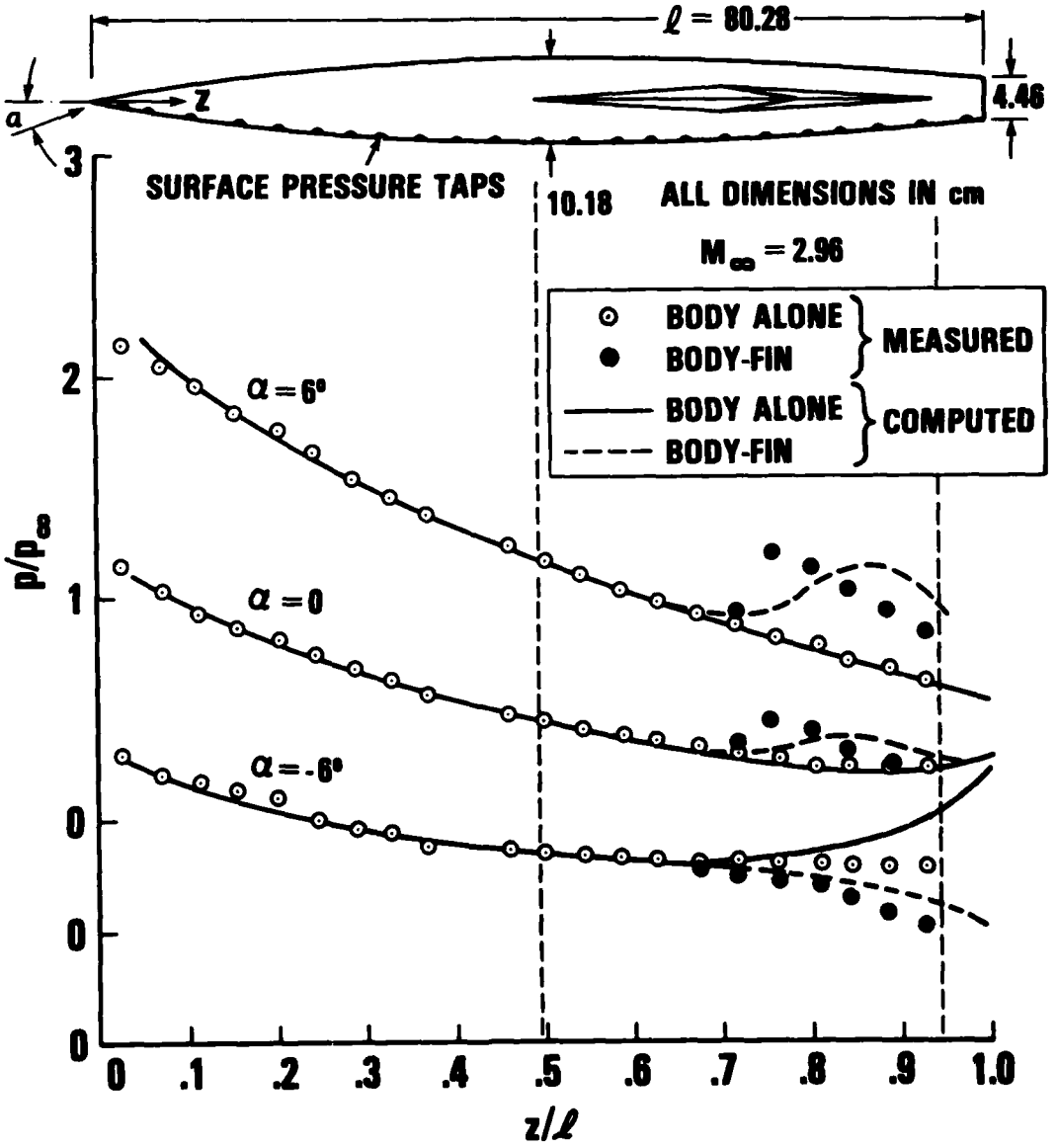

Figure 8. Calculated and measured body surface pressures with and without fins on the windward and leeward meridian at Mach 2.96.

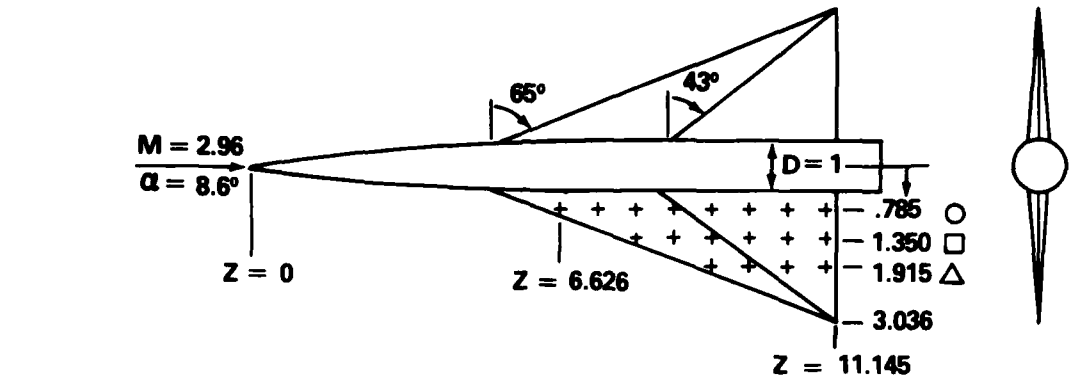

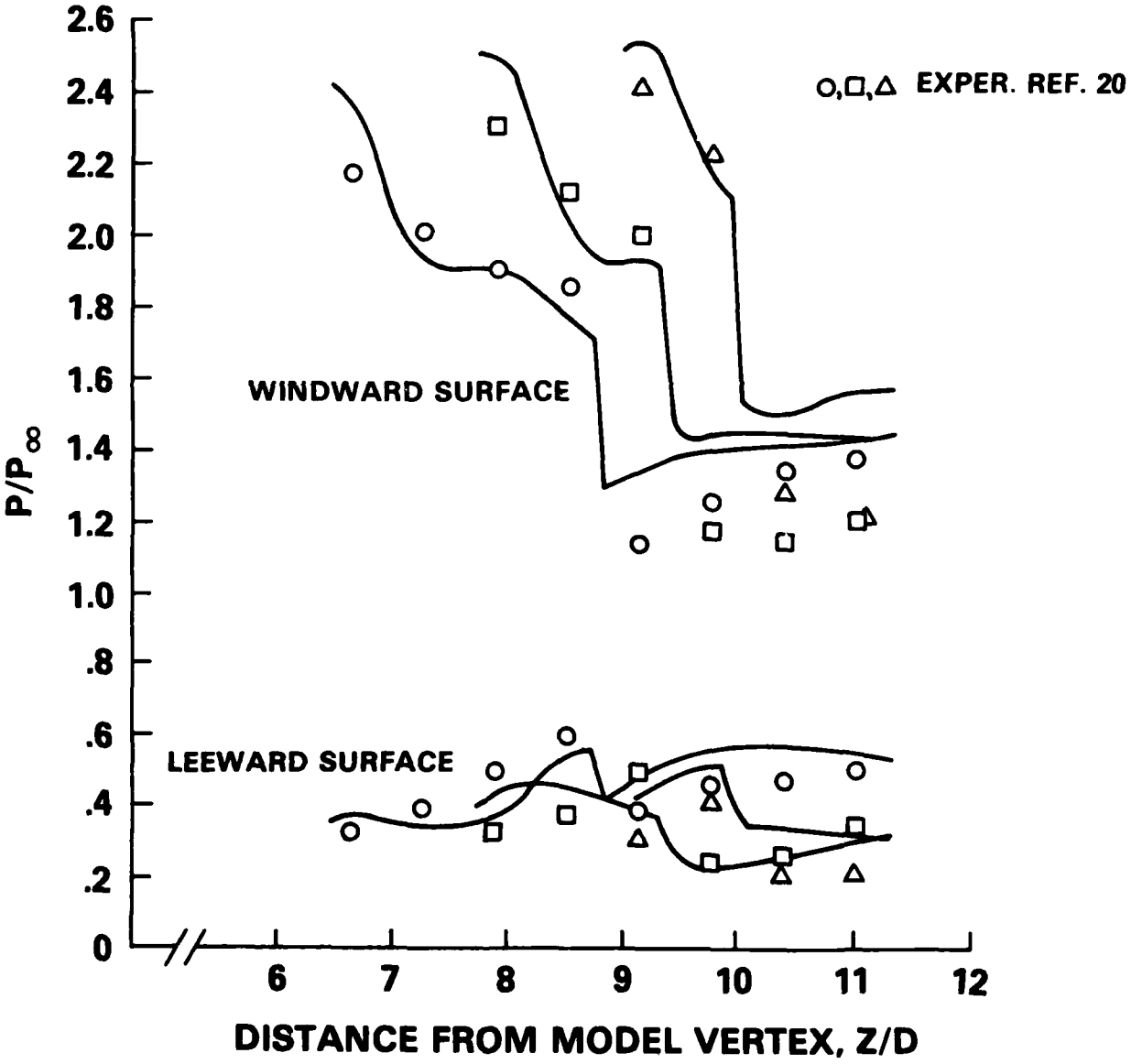

Figure 9. Comparison of computed and measured surface pressures at Mach 2.96 at $\alpha = 8.6$.

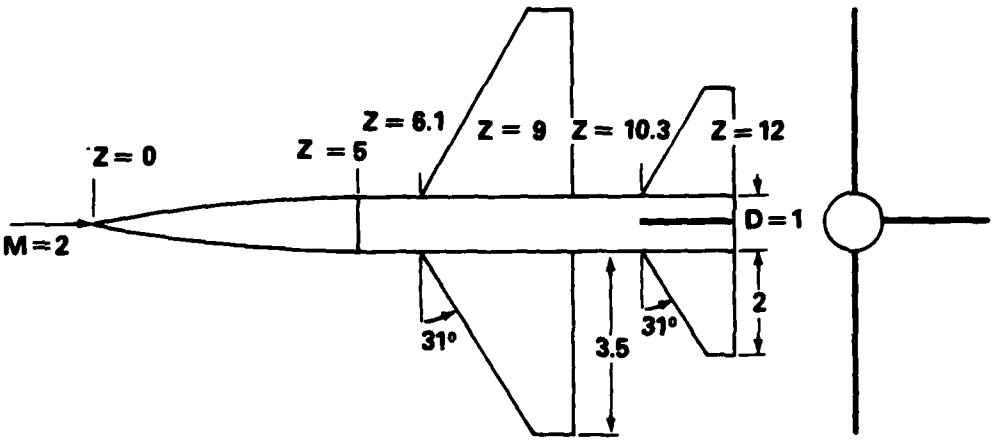

○ BODY – WING
◇ BODY – WING – TAIL } EXPERIMENT, REF. 21
●◆ COMPUTED

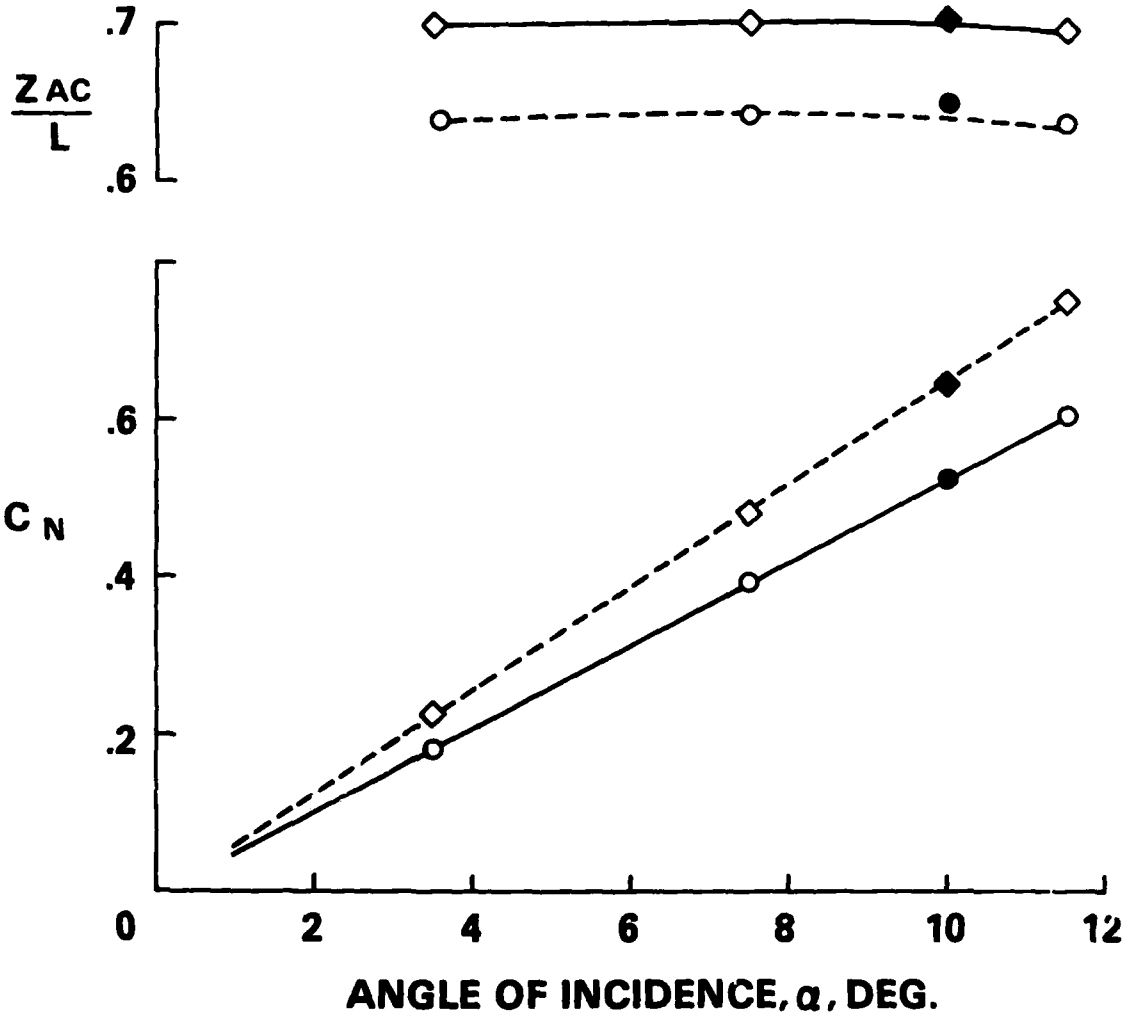

Figure 10. Measured and calculated normal force and center of pressure on a body-wing and body-wing-tail configurations at Mach 2.0.

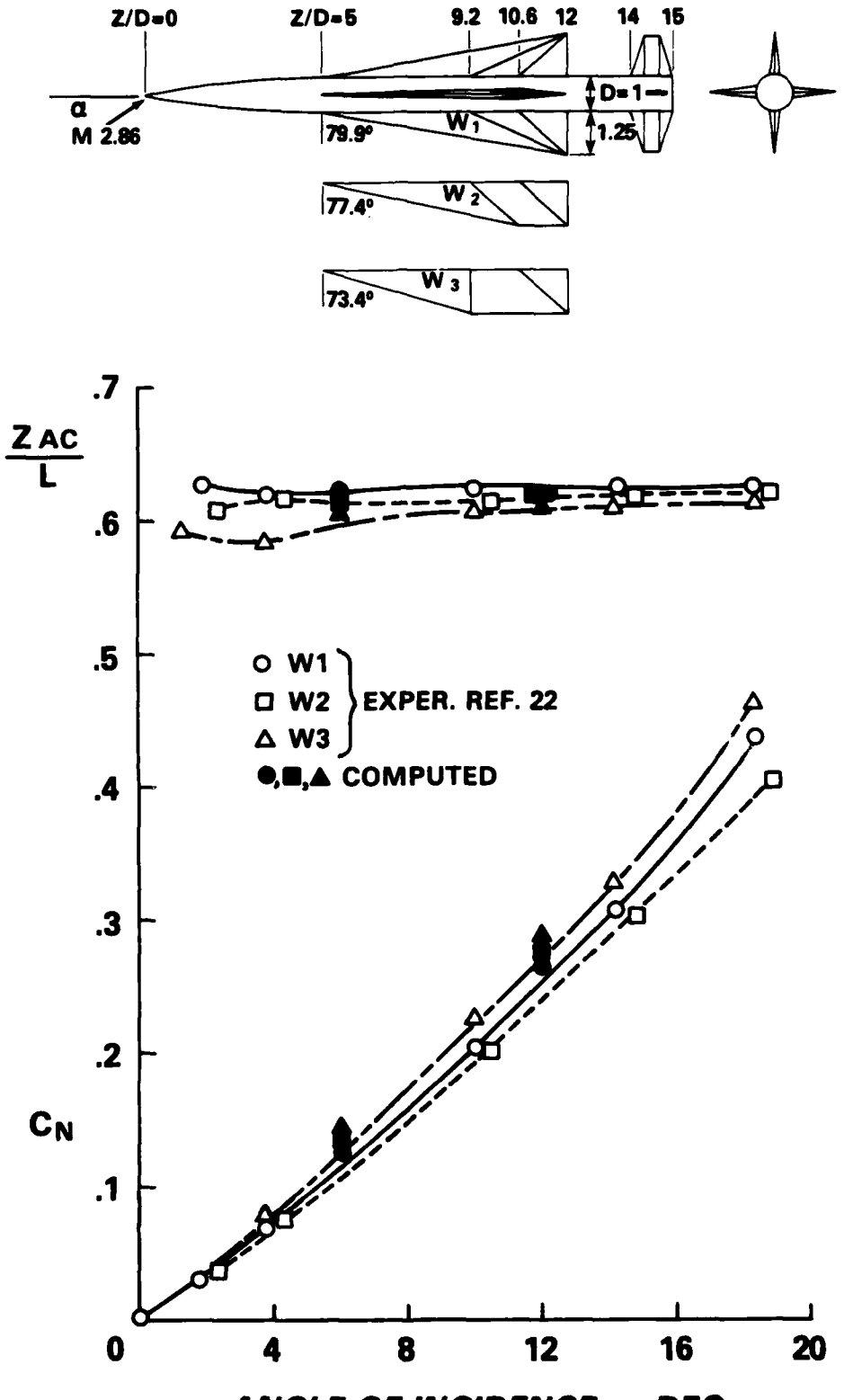

Figure 11. Measured and calculated normal force and center of pressure coefficients for three body-wing-tail configurations.
a. Tail not deflected ($\delta_T = 0$)

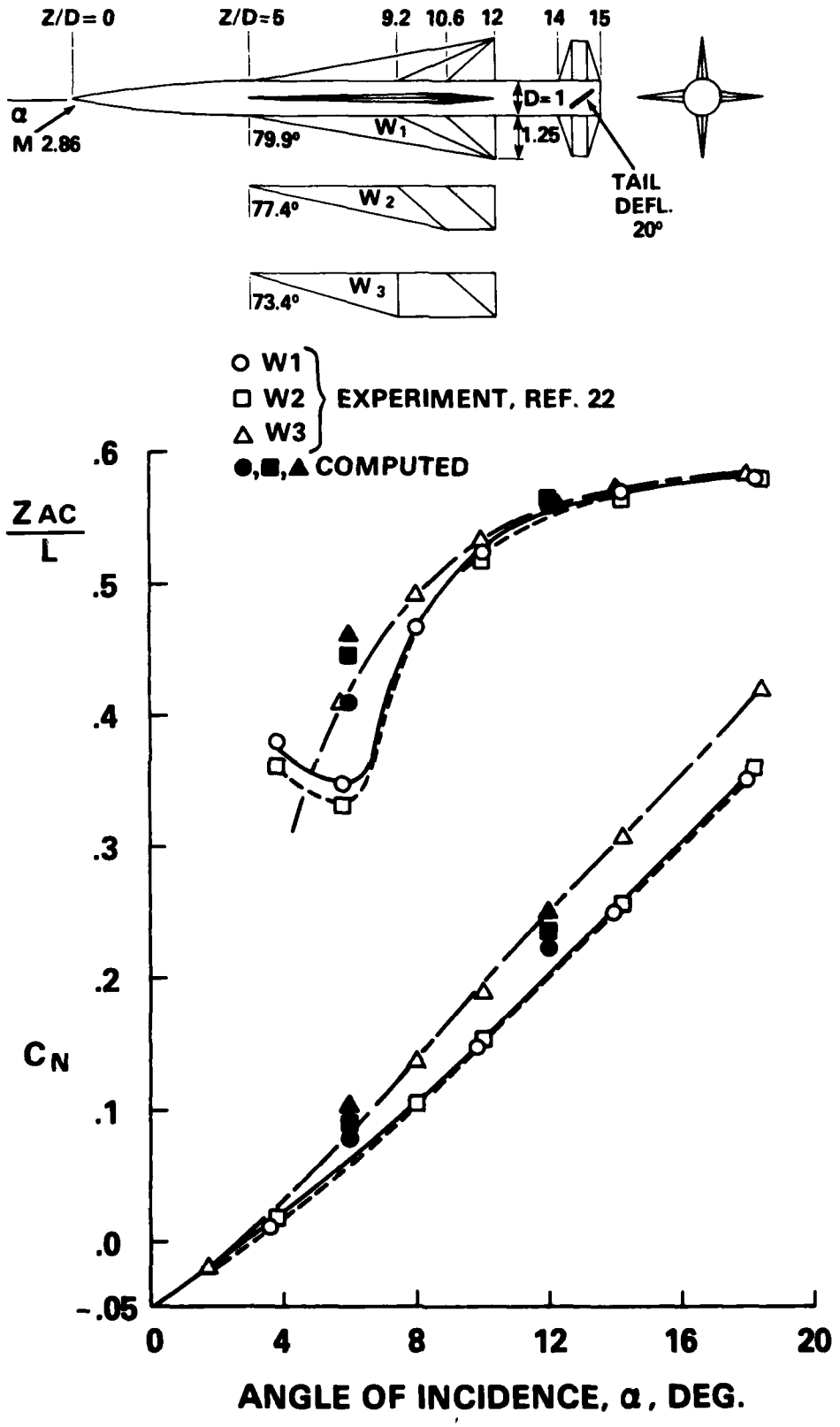

Figure 11. (Continued)

b. Tail deflected 20° (δ_T = -20°).

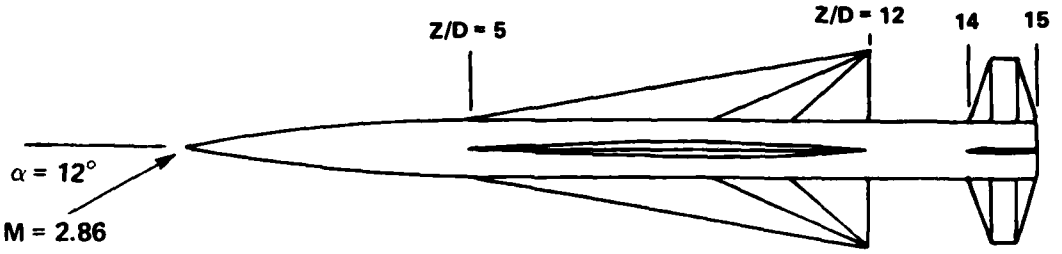

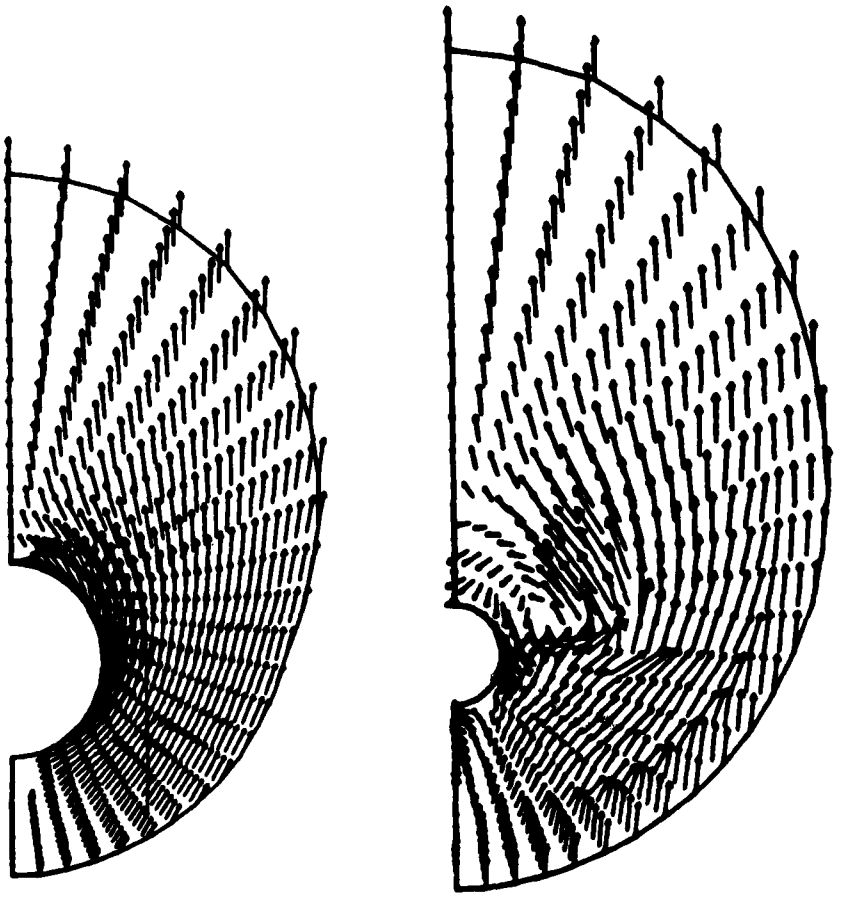

Z/D = 5 Z/D = 12

Figure 12. Calculated crossflow fields for the wing-body-tail configurations at several axial stations.

a. Z/D = 5 and Z/D = 12

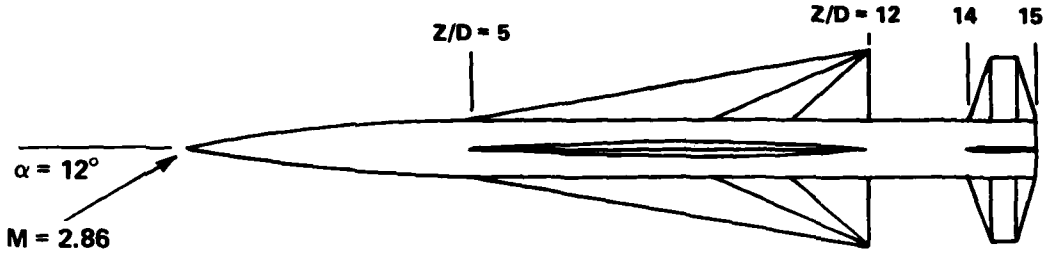

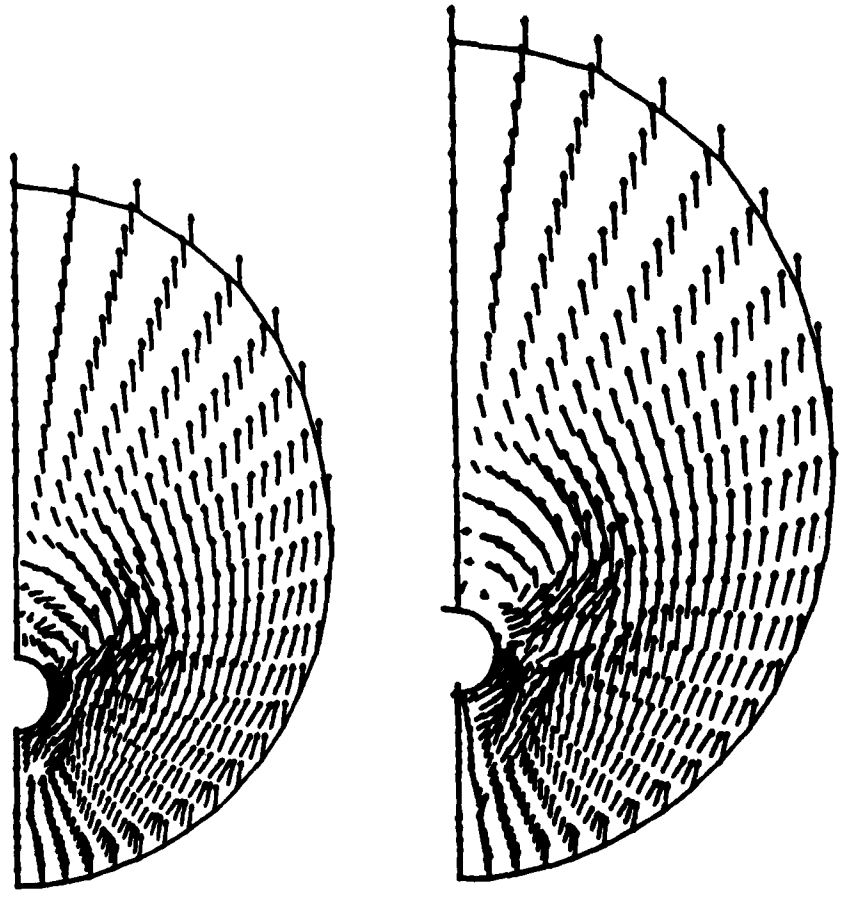

Z/D 14

Z/D = 15

Figure 12. (Continued)

b. Z/D = 14 and Z/D = 15

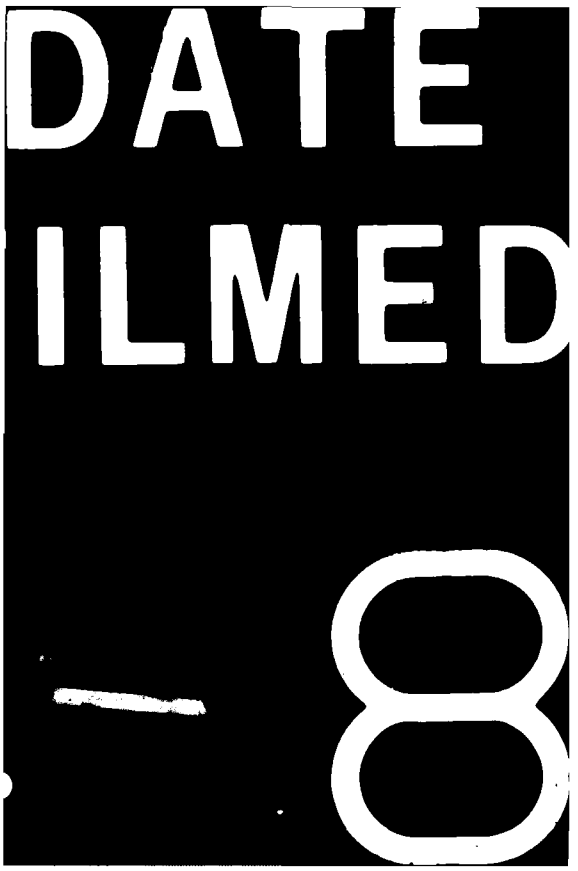
DATE
ILMED
8